Organic Electronics 15 (2014) 2285–2294

Contents lists available at ScienceDirect

Organic Electronics

journal homepage: www.elsevier.com/locate/orgel

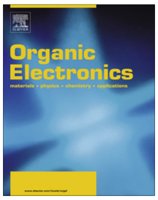

Open-circuit voltage up to 1.07 V for solution processed small molecule based organic solar cells

Wang Ni, Miaomiao Li, Bin Kan, Yi Zuo, Qian Zhang, Guankui Long, Huanran Feng,
Xiangjian Wan *, Yongsheng Chen *

Key Laboratory of Functional Polymer Materials, Collaborative Innovation Center of Chemical Science and Engineering (Tianjin), Center for Nanoscale Science and Technology, Institute of Polymer Chemistry, College of Chemistry, Nankai University, Tianjin 300071, China

ARTICLE INFO

Article history:
Received 8 April 2014
Received in revised form 8 June 2014
Accepted 9 June 2014
Available online 3 July 2014

Keywords:
Solution-processed small molecule
Organic photovoltaic cell
Open-circuit voltage
HOMO energy level
Thermal annealing

ABSTRACT

With the goal of increasing the open-circuit voltage, two new solution-processable A–D–A structure small molecule donor materials, named DCAO3TF and DCAO3TCz, using two weak electron-donating units, fluorene and carbazole as the central block have been designed and synthesized for photovoltaic applications. While bulk heterojunction photovoltaic devices based on DCAO3TF:$PC_{61}BM$ and DCAO3TCz:$PC_{61}BM$ as the active layers exhibit moderate power conversion efficiencies of 2.38% and 3.63%, respectively, devices based on DCAO3TF:$PC_{61}BM$ do exhibit an impressively high open-circuit voltage (V_{oc}) up to 1.07 V, which is one of the highest V_{oc} in organic solar cells based on donor:PCBM blend films.

1. Introduction

Organic photovoltaic (OPV) cells, as a promising alternative to traditional silicon solar cells, have attracted more and more attention due to their advantages of solution processability, low cost, light-weight, and flexibility [1–8]. In the past decade, great efforts have focused on the improvement of the power conversion efficiencies (PCEs) ($PCE = V_{oc} \times J_{sc} \times FF/P_{in}$) of bulk heterojunction (BHJ) structure OPV devices by addressing the factors that could simultaneously increase the three parameters open-circuit voltage (V_{oc}), short-circuit current (J_{sc}), and fill factor (FF), especially J_{sc} and FF. V_{oc} is highly correlated with the energy level difference between the highest occupied molecular orbital (HOMO) of the donor and the lowest unoccupied molecular orbital (LUMO) of the acceptor for polymer-based BHJ solar cells [9–11]. Many promising low band gap polymers designed for the efficient absorption of sunlight have been reported, and versatile strategies have been proposed to optimize the device fabrication. Recently, PCEs above 9% have been achieved for polymer-based OPVs (P-OPVs) [12–14]. Meanwhile, solution-processed small molecule based OPVs (SM-OPVs) have also stimulated great attention, due to their advantages of less batch-to-batch variation, easier band structure control, etc. [15–20]. Recently, PCEs of 8–9% [21–26] have been achieved for SM-OPVs, which are comparable to those of the best P-OPVs. It is worth noting that the V_{oc} of SM-OPV devices is usually higher than that of polymers from the statistical values reported in the literature [9,11,23–24,27]. The V_{oc} rule mentioned above seems also to work for SM BHJ solar cells, though no comprehensive studies have been devoted to this. In view of the defined chemical structures of small molecules and thus their easier controllable energy levels, it is more realistic to obtain a high V_{oc} for SM-OPV devices through tuning the HOMO energy level of the donor. This strategy could not only be useful to improve the OPV performance of single cells,

---

* Corresponding authors. Fax: +86 (22) 2349 9992.
E-mail addresses: xjwan@nankai.edu.cn (X. Wan), yschen99@nankai.edu.cn (Y. Chen).

http://dx.doi.org/10.1016/j.orgel.2014.06.012
1566-1199/

but could also be a valuable approach for tandem solar cells.

In our previous work, we have reported a series of linear acceptor–donor–acceptor (A–D–A) small molecules containing alkyl cyanoacetate terminal units and different cores such as thiophene dithieno[3,2-b:2',3'-d] silole (DTS) [28] and benzo[1,2-b:4,5-b'] dithiophene (BDT) [29]. The OPV devices using these molecules as donors have a V_{oc} in the range 0.80–0.95 V. Based on these studies, the HOMO energy level of A–D–A small molecules is mainly determined by the donor unit [30]. A–D–A small molecules using weak electron-donating units with a low HOMO energy level as the cores of a small molecule donor could generate an increased V_{oc} in OPV devices as in many cases for P-OPV devices [9,31–33]. Thus, in this work, we designed and synthesized two A–D–A structure small molecules, named DCAO3TF and DCAO3Cz with fluorene and carbazole as the central building blocks (Scheme 1), which exhibit a weak electron donating ability due to their low HOMO energy levels [31–36]. Their photovoltaic performance as well as other properties were studied and compared. OPV devices based on DCAO3TF:$PC_{61}BM$ and DCAO3TCz:$PC_{61}BM$ as active layers exhibit PCEs of 2.38% and 3.63%, respectively, and as expected, the devices based on DCAO3TF:$PC_{61}BM$ show an impressively high V_{oc} of 1.07 V, one of the highest values of V_{oc} in donor:PCBM-based bulk heterojunction OPVs.

2. Experimental section

2.1. General procedures and materials

All reactions and manipulations were carried out under an argon atmosphere using standard Schlenk techniques. All starting materials were purchased from commercial suppliers and used without further purification.

2.2. Synthesis of DCAO3TF and DCAO3TCz

The synthesis routes of DCAO3TF and DCAO3TCz are shown in Scheme 2. Compounds **1**–**3** were synthesized according to the literature [28,32,37].

2.2.1. Synthesis of compound **4**

A solution of compounds **1** (1.1 g, 1.71 mmol) and **3** (2.2 g, 3.79 mmol) in toluene (45 mL) and aqueous 1 M Na_2CO_3 (15 mL) was degassed twice with argon. Then $Pd(PPh_3)_4$ (30 mg, 0.026 mmol) was added and the mixture was stirred at 100 °C for 24 h under argon, after which the mixture was poured into water (200 mL), and extracted with chloroform. The organic layer was washed with water, and then dried over anhydrous Na_2SO_4. The solvent was removed by a rotating evaporator and the residue was purified by silica gel chromatography using a mixture of petroleum ether and dichloromethane (1:1) eluant to produce compound **4** (1.4 g, 59%). ^1H NMR (400 MHz, $CDCl_3$): δ 9.83 (s, 2H), 7.67(d, J = 7.6 Hz, 2H), 7.60 (s, 2H), 7.56 (d, J = 7.6 Hz, 2H), 7.55 (s, 2H), 7.27(d, J = 3.6 Hz, 2H), 7.25 (s, 2H), 7.16 (d, J = 3.6 Hz, 2H), 2.85 (m, 8H), 2.05 (m, 4H), 1.72 (m, 8H), 1.30 (m, 40H), 1.08 (m, 20H), 0.89 (t, 12H), 0.80 (t, 6H), 0.70 (m, 4H). ^{13}C NMR (100 MHz, $CDCl_3$): δ182.51, 151.76, 143.30, 141.40, 141.15, 140.43, 140.24, 140.13, 139.12, 138.51, 134.31, 132.74, 129.08, 127.85, 126.10, 125.96, 124.64, 120.19, 119.67, 55.34, 40.41, 31.92, 31.88, 31.81, 30.71, 30.32, 29.97, 29.79, 29.72, 29.50, 29.43, 29.33, 29.27, 29.21, 23.74, 22.69, 22.60, 14.13, 14.08. MS (MALDI-TOF): calcd for $C_{87}H_{118}O_2S_6$ $[M^+]$, 1386.75; found:1386.72.

2.2.2. Synthesis of compound **5**

A solution of compounds **2** (0.85 g, 1.60 mmol) and **3** (2.0 g, 3.45 mmol) in toluene (45 mL) and aqueous 1 M Na_2CO_3 solution (15 mL) was degassed twice with argon, Then $Pd(PPh_3)_4$ (30 mg, 0.026 mmol) was added and the mixture was stirred at 100 °C for 24 h under argon. The mixture was then poured into water (200 mL), and extracted with chloroform. The organic layer was washed with water, and then dried over anhydrous Na_2SO_4. The solvent was removed by a rotating evaporator and the residue was purified by silica gel chromatography using a mixture of petroleum ether and dichloromethane (1:1) as eluant to produce compound **5** (1.2 g, 58%). ^1H NMR (400 MHz, $CDCl_3$): δ 9.82 (s, 2H), 8.02 (d, J = 8.0 Hz, 2H), 7.59 (s, 2H), 7.53 (s, 2H), 7.48 (d, J = 8.0 Hz, 2H), 7.26 (d, J = 4.0 Hz, 2H), 7.25 (s, 2H), 7.16 (d, J = 4.0 Hz, 2H), 4.30

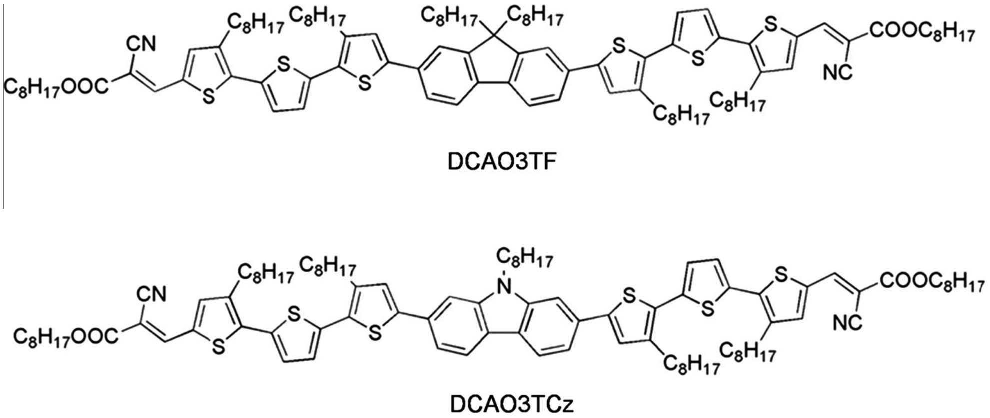

Scheme 1. Chemical structures of DCAO3TF and DCAO3TCz.

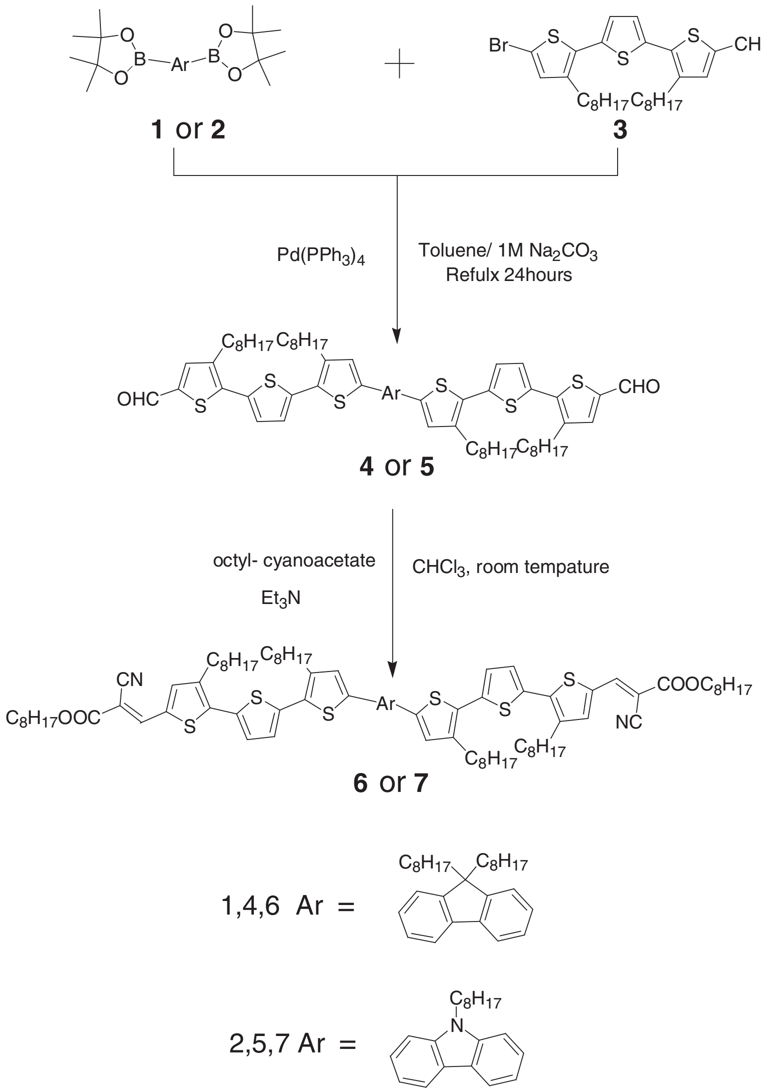

Scheme 2. Synthesis routes of DCAO3TF and DCAO3TCz.

(t, 2H), 2.83 (m, 8H), 1.92 (m, 2H), 1.72 (m, 8H), 1.30 (m, 50H), 0.89 (m, 15H). ^{13}C NMR (100 MHz,CDCl$_3$): δ 182.53, 143.78, 141.47, 141.37, 141.17, 140.23, 140.12, 139.12, 138.56, 134.27, 131.62, 129.15, 127.83, 126.28, 125.92, 122.37, 120.71, 117.47, 105.58, 31.92, 31.87, 30.67, 30.31, 29.82, 29.72, 29.51, 29.44, 29.34, 29.28, 29.22, 28.95, 27.24, 22.70, 14.13. MS (MALDI-TOF): calcd for $C_{78}H_{101}NO_2S_6$ [M$^+$], 1275.59; found:1275.62.

*2.2.3. Synthesis of compound **6** (DCAO3TF)*

Compound **4** (0.30 g, 0.216 mmol) was dissolved in a solution of dry CHCl$_3$ (60 mL), then octyl-cyanoacetate (0.6 ml, 3.26 mmol) and three drops of triethylamine were added, the resulting solution was refluxed and stirred for 12 h under argon. The solvent was then removed by a rotating evaporator and the crude product was dissolved in 10 mL of chloroform, then precipitated from methanol and the precipitate was filtered off. The residue was purified by silica gel chromatography using a mixture of petroleum ether and chloroform (2:1) as eluant, and the crude solid was recrystallized from a hexane and chloroform mixture three times to produce compound **6** (0.16 g, 42%). ^{1}H NMR (400 MHz, CDCl$_3$): δ 8.21 (s, 2H), 7.68 (d, J = 7.6 Hz, 2H), 7.60 (s, 2H), 7.59 (d, J = 7.6 Hz, 2H), 7.55 (s, 2H), 7.33 (d, J = 7.6 Hz, 2H), 7.26 (s, 2H), 7.18 (d, J = 7.6 Hz, 2H), 4.29 (t, 4H), 2.83 (m, 8H), 2.06 (m, 4H), 1.72 (m, 12H), 1.30 (m, 60H), 1.08 (m, 20H), 0.89 (t, 18H), 0.80 (t, 6H), 0.70 (m, 4H). ^{13}C NMR (100 MHz, CDCl$_3$): δ162.14, 150.77, 144.94, 142.41, 140.82, 140.49, 139.81, 139.43,139.41, 137.98, 132.90, 131.85, 131.70, 128.06, 127.25, 125.12, 125.00, 123.61, 119.17, 118.69, 115.02, 96.60, 65.53, 54.33, 39.379, 30.891, 30.846, 30.781, 29.645, 29.222, 28.942, 28.793, 28.69, 28.52, 28.48, 28.39, 28.30, 28.25, 28.17, 27.54, 24.79, 22.70, 21.66, 21.58, 13.10, 13.05. MS (MALDI-TOF): calcd for $C_{109}H_{152}N_2O_4S_6$ [M$^+$], 1745.01; found:1745.01.

*2.2.4. Synthesis of compound **7** (DCAO3TCz)*

Compound **5** (0.30 g, 0.24 mmol) was dissolved in a solution of dry chloroform (60 mL), then octyl-cyanoacetate (0.6 ml, 3.26 mmol) and three drops of triethylamine were added, the mixture was refluxed and stirred for 12 h under argon. The solvent was then removed by a rotating evaporator and the crude product was dissolved in 10 mL of chloroform, then precipitated from methanol and the precipitate was filtered off. The residue was purified by silica gel chromatography using a mixture of petroleum ether and chloroform (2:1) as eluent and the crude solid was recrystallized from a hexane and chloroform mixture three times to produce compound **7** (0.32 g, 82%).^{1}H NMR (400 MHz, $CDCl_3$): δ 8.19 (s, 2H), 8.03 (d, *J* = 8.0 Hz, 2H), 7.58 (s, 2H), 7.54 (s, 2H), 7.49 (d, *J* = 8.0 Hz, 2H), 7.31 (d, *J* = 4.0 Hz, 2H),7.27 (s, 2H), 7.17 (d, *J* = 4.0 Hz, 2H), 4.35 (t, 2H), 4.28 (t, 4H), 2.84 (t, 8H), 1.93 (m, 2H), 1.72 (m, 12H), 1.43–1.28 (m, 70H), 0.89–0.83 (m, 21H). ^{13}C NMR (100 MHz, $CDCl_3$): δ163.16, 145.93, 143.89, 141.87, 141.48, 140.83, 140.38, 139.06, 133.87, 132.83, 131.60, 129.16, 128.23, 126.32, 125.96, 122.39, 120.72, 117.45, 116.06, 105.60, 97.54, 66.54, 31.92, 31.88, 31.78, 30.846, 30.62, 30.23, 29.86, 29.71, 29.56, 29.53, 29.43, 29.34, 29.29, 29.20, 28.96, 28.57, 27.25, 25.81, 22.66, 14.13. MS (MALDI-TOF): calcd for $C_{100}H_{135}N_3O_4S_6$ [M^+], 1633.88; found:1633.86.

2.3. Measurements and instruments

The ^{1}H and ^{13}C nuclear magnetic resonance NMR spectra were taken on a Bruker AV400 Spectrometer. Matrix assisted laser desorption/ionization time-of-flight mass spectrometry (MALDI-TOF MS) was performed on a Bruker Autoflex III instrument. Transmission electron microscopy (TEM) was performed on a Philips Technical G^2 F20 at 200 kV. Thermogravimetric analyses (TGA) were carried out on a NETZSCH STA 409PC instrument under a purified nitrogen gas flow with a 10 °C min^{-1} heating rate. UV–vis spectra were obtained with a JASCO V-570 spectrophotometer. X-ray diffraction (XRD) experiments were performed on a Bruker D8 FOCUS X-ray diffractometer with Cu Kα radiation (λ = 1.5406 Å) at a generator voltage of 40 kV and a current of 40 mA. Atomic force microscope (AFM) investigation was performed using a Bruker MultiMode 8 instrument in the "tapping" mode. Cyclic voltammetry (CV) experiments were performed with a LK98B II Microcomputer-based Electrochemical Analyzer in dichloromethane solutions. All measurements were carried out at room temperature with a conventional three-electrode configuration using a glassy carbon electrode as the working electrode, a saturated calomel electrode (SCE) as the reference electrode, and a Pt wire as the counter electrode. The dichloromethane was distilled from calcium hydride under dry argon immediately prior to use. Tetrabutylammonium phosphorus hexafluoride (Bu_4NPF_6, 0.1 M) in dichloromethane was used as the supporting electrolyte, and the scan rate was 100 mV s^{-1}. Ultraviolet photon spectroscopy (UPS) was measured using a VG Scienta High UPS system with the He (I) (21.2 eV) line using a negative bias voltage applied to the samples in order to shift the spectra from the spectrometer threshold.

The current density–voltage (*J*–*V*) characteristics of photovoltaic devices were obtained by a Keithley 2400 source-measure unit. The photocurrent was measured under simulated illumination of 100 mW cm^{-2} with AM1.5G irradiation using a xenon-lamp-based solar simulator [Oriel 96000 (AM1.5G)] in an argon-filled glove box. Simulator irradiance was characterized using a calibrated spectrometer, and illumination intensity was set using a certified silicon diode. External quantum efficiency values (EQEs) of the encapsulated devices were obtained with a halogen-tungsten lamp, monochromator, optical chopper, and lock-in amplifier in air and the photon flux was determined by a calibrated silicon photodiode.

Hole mobility was measured by space charge limited current (SCLC) method using a diode configuration of ITO/PEDOT:PSS/donor:$PC_{61}BM$/Au by taking the dark current density in the range of 0–6 V and fitting the results to a space charge limited form, where SCLC is described by:

$$\ln\frac{JL^3}{V^2} = \ln\left(\frac{9}{8}\varepsilon_r\varepsilon_0\mu_0\right) + 0.89\beta\sqrt{\frac{V}{L}} = k\sqrt{\frac{V}{L}} + C$$
$$k = 0.89\beta;\, C = \ln\left(\frac{9}{8}\varepsilon_r\varepsilon_0\mu_0\right)$$

where *J* is the current density, *L* is the film thickness of the active layer, μ_0 is the hole mobility, ε_r is the relative dielectric constant of the transport medium, ε_0 is the permittivity of free space (8.85×10^{-12} F m^{-1}), V (=$V_{\mathrm{appl}} - V_{\mathrm{bi}}$) is the internal voltage of the device, where V_{appl} is the applied voltage to the device and V_{bi} is the built-in voltage due to the relative work function difference of the two electrodes.

2.4. Fabrication of organic solar cells

The photovoltaic devices were fabricated with a structure of glass/ITO/PEDOT:PSS/donor:acceptor/ZnO/Al. The ITO-coated glass substrates were cleaned by ultrasonic treatment in detergent, deionized water, acetone, and isopropyl alcohol under ultrasonication for 15 min each time and subsequently dried by a nitrogen flow. A thin layer of PEDOT:PSS (Baytron P VP AI 4083, filtered at 0.45 μm) was spin-coated (3000 rpm, ca. 40 nm thick) onto the ITO surface. After baking at 150 °C for 20 min, the substrates were

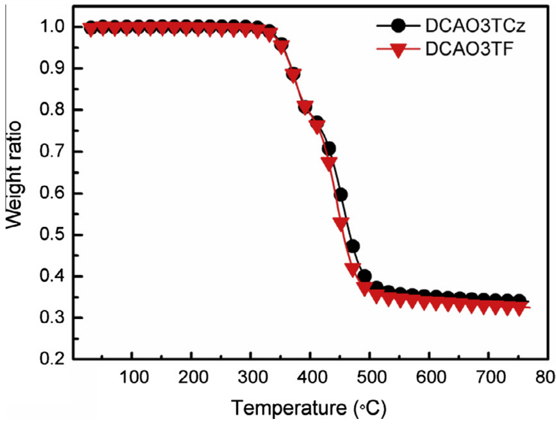

Fig. 1. TGA curves of DCAO3TF and DCAO3TCz with a heating rate of 10 °C/min under N_2 atmosphere.

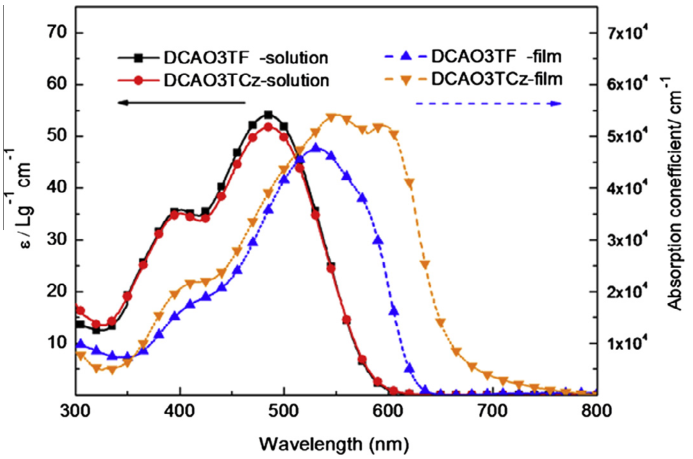

Fig. 2. Absorption spectra of DCAO3TF and DCAO3TCz in chloroform solution and as-cast film.

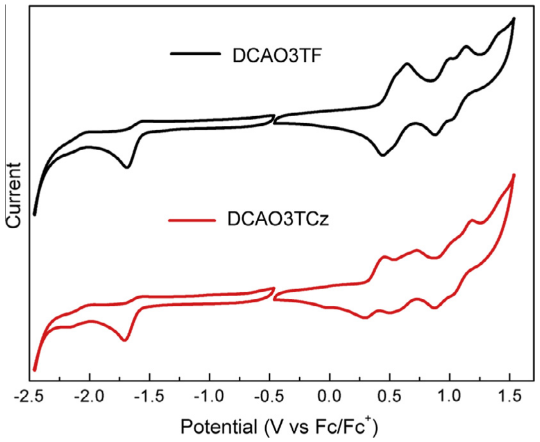

Fig. 3. Cyclic voltammograms of DCAO3TF and DCAO3TCz in a dichloromethane solution of 0.1 mol L^{-1} Bu_4NPF_6 with a scan rate of 100 mV s^{-1}.

transferred into an argon-filled glove box. The active layer was then spin-cast from different blend ratios (w:w) of donor materials (8 mg mL^{-1}) and $PC_{61}BM$ in chloroform solution at 1700 rpm for 20 s on the ITO/PEDOT:PSS substrate. Subsequently, a ZnO particle suspension obtained by the sol–gel method [38] was spin-cast on top of the active layer. After the ZnO spin coating, thermal annealing was carried out on a digitally controlled hotplate at various temperatures in an argon-filled glove box. Finally, a 50 nm Al layer was deposited on the ZnO film under high vacuum ($<2 \times 10^{-4}$ Pa). The thicknesses of the ZnO and active layers were measured using Dektak 150 profilometer. The effective area of each cell was 4 mm^2 as defined by masks.

3. Result and discussion

3.1. Synthesis and thermal properties

As shown in Scheme 2, the intermediates of dialdehyde 4 and 5 were synthesized from Suzuki coupling in refluxing toluene for 24 h, using Na_2CO_3 as the base under an argon atmosphere in the presence of Aliquat336 and $Pd(PPh_3)_4$ as the catalyst. The target molecules were then prepared by

Table 1
Optical and electrochemical data of DCAO3TF and DCAO3TCz.

Compound	$\lambda_{max,sol}$ (nm)	ε_{sol} (Lg^{-1} cm^{-1})	$\lambda_{max,film}$ (nm)	ε_{film} (cm^{-1})	$E_g^{opt,film}$ (eV)	E_g^{CV} (eV)	IP^{UPS} (eV)	HOMO^{CV} (eV)	LUMO^{CV} (eV)
DCAO3TF	485	54	529	5.4×10^4	2.01	2.0	5.69	−5.23	−3.23
DCAO3TCz	485	51	536	5.7×10^4	1.92	1.94	5.61	−5.14	−3.21

Table 2
Current density–voltage characteristics of the optimized SM OPV devices.

Donor:$PC_{61}BM$ (w:w)	V_{oc} (V)	J_{sc} (mA cm^{-2})	FF	PCE$_{best}$ (%)	PCE$_{ave}$ (%)
DCAO3TF:$PC_{61}BM$ (1:0.8)[a]	1.07	3.93	0.45	1.89	1.67(±0.22)[c]
DCAO3TF:$PC_{61}BM$ (1:0.8)[b]	1.07	4.54	0.49	2.38	2.21(±0.17)[c]
DCAO3TCz:$PC_{61}BM$ (1:0.8)[a]	0.97	4.28	0.58	2.41	2.23(±0.18)[c]
DCAO3TCz:$PC_{61}BM$ (1:0.8)[b]	0.97	6.15	0.61	3.63	3.48(±0.15)[c]

[a] Without annealing.
[b] Thermal annealing at 80 °C for 10 min.
[c] Average over 20 devices.

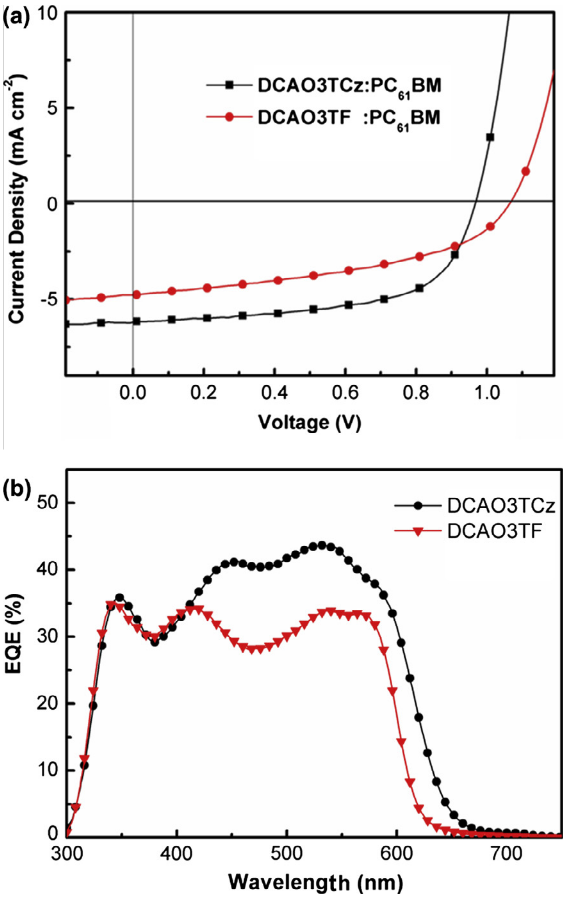

Fig. 4. (a) *J–V* curves of DCAO3TF:$PC_{61}BM$ (1:0.8, w/w) and DCAO3TCz:$PC_{61}BM$ (1:0.8, w/w) after thermal annealing at 80 °C for 10 min and (b) EQE of the devices based on DCAO3TF:$PC_{61}BM$ (1:0.8, w/w) and DCAO3TCz:$PC_{61}BM$ (1:0.8, w/w) after thermal annealing at 80 °C for 10 min.

Knoevenagel condensation of 4 or 5 with octyl-cyanoacetate. TGA indicates that DCAO3TF (compound **6**) and DCAO3TCz (compound **7**) exhibit good thermal stability up to 350 °C under a N_2 atmosphere (see Fig. 1).

3.2. Optical properties and electrochemical properties

The UV–vis absorption spectra of DCAO3TF and DCAO3TCz in a dilute chloroform solution and in the solid state are shown in Fig. 2. DCAO3TF in chloroform shows a maximum absorption peak at 485 nm with a maximum absorption coefficient of 54 L g^{-1} cm^{-1}. In the solid state, a red shifted maximum absorption peak is observed at 532 nm for the DCAO3TF as-cast film with a maximum absorption coefficient of 4.7×10^4 cm^{-1}. The DCAO3TCz solution also shows an maximum absorption peak at 485 nm with a comparable absorption coefficient of 51 L g^{-1} cm^{-1}. Compared with DCAO3TF, the as-cast DCAO3TCz film shows a broader absorption and a red-shifted maximum absorption peak at 551 nm with a higher maximum absorption coefficient of 5.4×10^4 cm^{-1}. The optical band gaps of DCAO3TF and DCAO3TCz are estimated to be 2.01 and 1.92 eV from the onset of the film absorption spectra.

The electrochemical properties of DCAO3TF and DCAO3TCz were investigated by cyclic voltammetry (CV). Ferrocene/ferrocenium of the (Fc/Fc^+) redox couple (4.8 eV below the vacuum level) was used as the internal calibration. As shown in Fig. 3, the HOMO energy levels and LUMO energy levels, which are respectively −5.23 and −3.23 eV for DCAO3TF, and −5.14 and −3.21 eV for DCAO3TCz, are calculated based on the onset oxidation potential and the onset reduction potential of the redox curves. Note that DCAO3TF exhibits a deeper HOMO energy level (−5.23 eV) compared to DCAO3TCz (−5.14 eV), but the LUMO energy levels of DCAO3TF and DCAO3TCz are very similar (~−3.20 eV), which are predominantly determined by the acceptor unit [30]. The electrochemical band gaps of DCAO3TF and DCAO3TCz are estimated to be 2.0 and 1.94 eV. The results are consistent with the optical data. The ionization energies (IP) of DCAO3TF and DCAO3TCz have been respectively

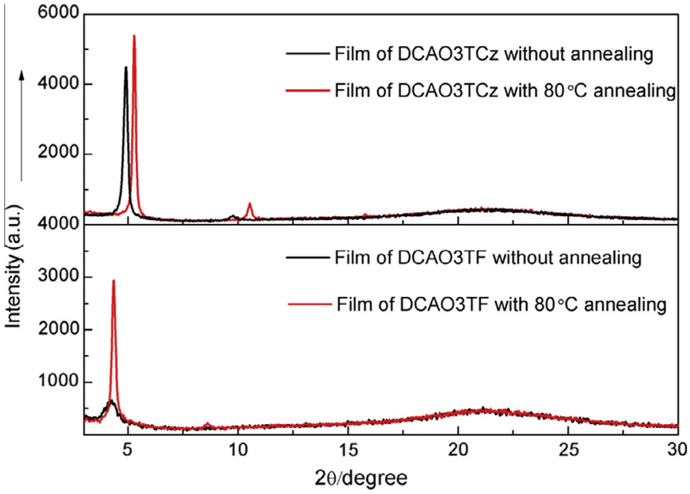

Fig. 5. XRD patterns of DCAO3TF and DCAO3TCz films spin-coated from $CHCl_3$ onto a glass substrate.

determined to be −5.69 and −5.61 eV by UPS. These values are comparable to the reported results of other similar A–D–A structure molecules [39]. The difference between solid state UPS and the solution CV results may be due to the aggregation from solution to film states [40]. Some important optical and electrochemical properties of the two molecules are listed in Table 1.

Table 3
Hole mobilities of the films of these two molecules blended with $PC_{61}BM$.

Donor:$PC_{61}BM$(w:w)	Hole mobility ($cm^2\ V^{-1}\ s^{-1}$)
DCAO3TF:$PC_{61}BM$(1:0.8)[a]	5.19×10^{-5}
DCAO3TF:$PC_{61}BM$(1:0.8)[b]	1.12×10^{-4}
DCAO3TCz:$PC_{61}BM$(1:0.8)[a]	6.47×10^{-5}
DCAO3TCz:$PC_{61}BM$(1:0.8)[b]	1.62×10^{-4}

[a] Without annealing.
[b] After thermal annealing at 80 °C for 10 min.

3.3. Photovoltaic performance

BHJ organic solar cells were fabricated using DCAO3TF and DCAO3TCz as the electron donor materials and $PC_{61}BM$ as the electron acceptor material with a device structure of glass/ITO/PEDOT:PSS/donor:acceptor/ZnO/Al, using the conventional solution spin-coating process. The corresponding optimized parameters with a donor:acceptor ratio 1:0.8 (w/w) are summarized in Table 2. The optimum current density vs voltage (*J*–*V*) curves measured under AM 1.5G illumination at an intensity of 100 mW cm^{-2} are shown in Fig. 4a. For DCAO3TF without annealing, the best PCE of 1.89% was obtained with a V_{oc} value as high as 1.07 V, a J_{sc} of 3.93 mA cm^{-2} and a FF of 0.45. The devices based on DCAO3TCz showed a V_{oc} of 0.97 V, a J_{sc} of 4.28 mA cm^{-2} and a FF of 0.58 with the best PCE of 2.41%. After thermal annealing at 80 °C for 10 min, the best PCEs increased to 2.38% for DCAO3TF and 3.63% for DCAO3TCz, which are attributed to increase in both J_{sc} and FF as shown in Table 1. The effect of thermal annealing on the improved performance will be discussed in detail in the following section. Note that the devices using both donor molecules exhibit a high V_{oc}, with the device using DCAO3TF showing an impressively high V_{oc} up to 1.07 V, which is one of the highest V_{oc} values reported for organic solar cells using PCBM as the acceptor. Also, the DCAO3TCz-based device shows a high V_{oc} of 0.97 V. Obviously, the high V_{oc} of the devices based on the two small molecules is attributed to their low HOMO energy levels. According to the results of CV and UPS in Table 1, the higher V_{oc} for DCAO3TF devices is consistent with its lower HOMO energy level compared with that of DCAO3TCz. Note, the HOMO energy levels of these two molecules are lower than those of molecules with similar backbone

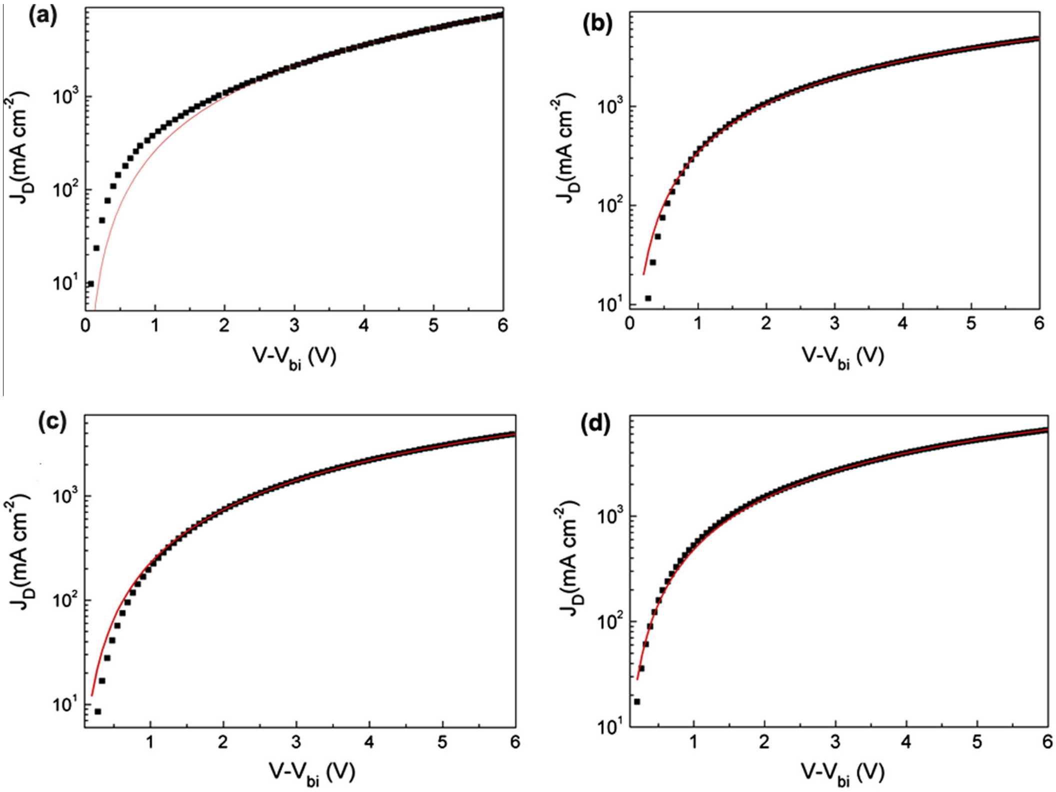

Fig. 6. *J*–*V* characteristics of a hole-only device with the configuration ITO/PEDOT:PSS (30 nm)/Donor:$PC_{61}BM$ without ETL/Au (30 nm). (a and b) device based on DCAO3TF:$PC_{61}BM$, (c and d) device based on DCAO3TCz:$PC_{61}BM$. (a and c) no annealing and (b and d) annealing at 80 °C for 10 min. The solid lines represent the fit using a model of single carrier SCLC with field-independent mobility. The J_D–V characteristics are corrected for the built-in voltage V_{bi} that arises from the work function difference between the contacts.

structures but different central building blocks (−4.96 eV [28] and −5.04 eV [29]), reported in our previous studies, which is consistent with the lower V_{oc} of the earlier molecules. These results indicate that the approach using central building blocks with weaker electron donating ability could indeed lower the HOMO energy levels of the molecules and thus improve the V_{oc} of devices based on these molecules. EQE spectra of the optimized devices

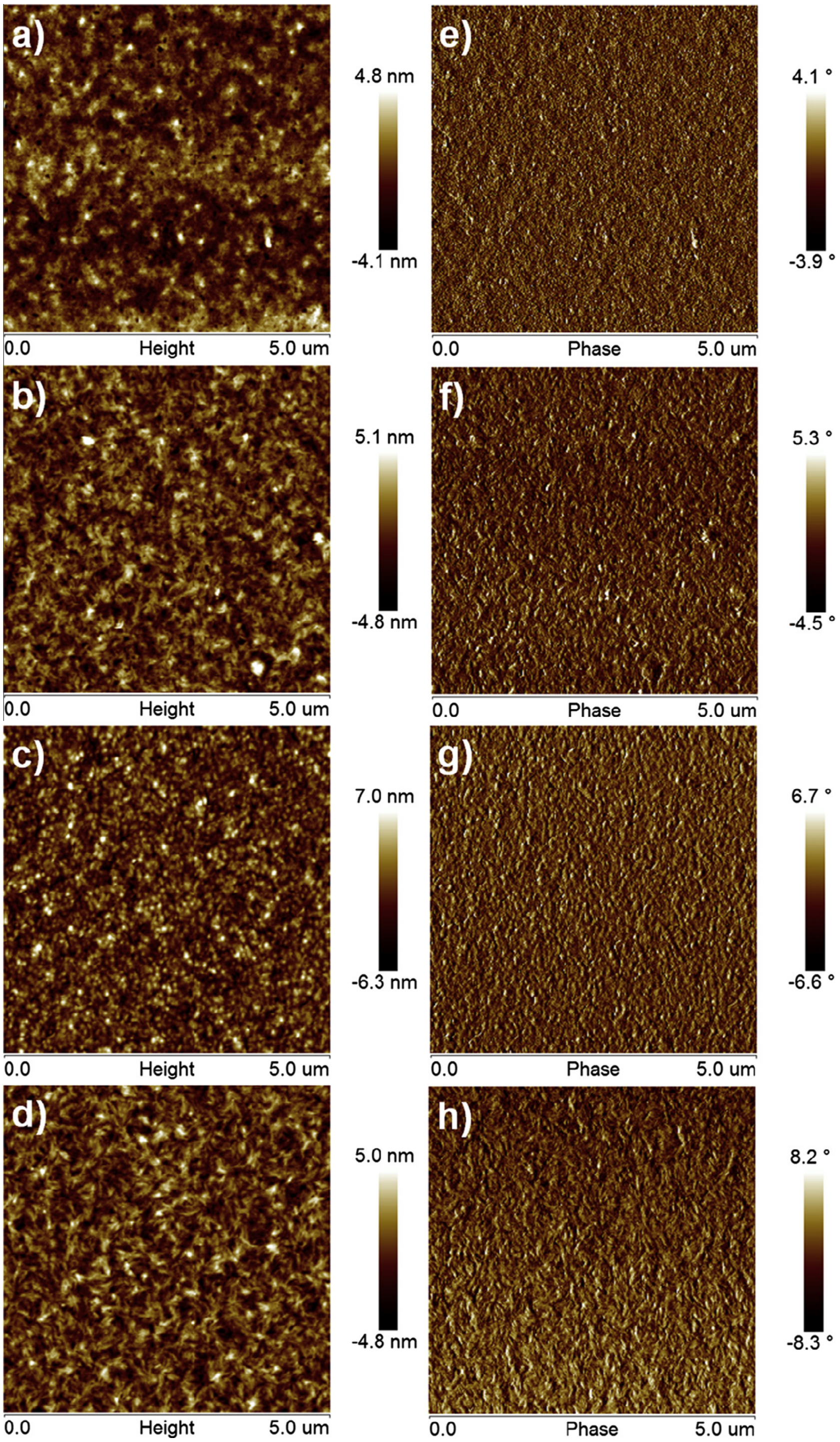

Fig. 7. (a–d) Tapping-mode AFM height images and (e–h) phase images of the active layers with DCAO3TF/$PC_{61}BM$ (1:0.8,w/w) (a and e) no annealing and (b and f) after thermal annealing at 80 °C for 10 min, DCAO3TCz/$PC_{61}BM$(1:0.8,w/w) (c and g) no annealing and (d and h) after thermal annealing at 80 °C for 10 min.

based on the new molecules are shown in Fig. 4b, where devices based on DCAO3TF and DCAO3TCz exhibited photo-to-current responses from 300 to 650 nm with the maximum EQE values reaching 34% and 43%, respectively. The calculated J_{sc} integrated from EQE for optimum devices is 4.28 mA cm^{-2} for DCAO3TF and 5.77 mA cm^{-2} for DCAO3TCz, pretty close to the J–V measurement shown in Fig. 4a.

3.4. Analysis of the impact of thermal annealing on morphology and device performance

To understand the impact of thermal annealing on the device performance, several structural analysis methods were used to analyze morphology of the active layers. According to the XRD results shown in Fig. 5, DCAO3TF exhibited a weak diffraction peak (100) at $2\theta = 4.25°$ indicating poor stacking of the film spin-coated from chloroform. But after thermal annealing at 80 °C for 10 min, a significantly increased intensity (100) diffraction peak at $2\theta = 4.35°$ and a second-order diffraction peak at $2\theta = 8.62°$ were observed, which indicated better organized assembly and crystallinity of DCAO3TF were produced after thermal annealing. For the DCAO3TCz case, a strong diffraction peak at $2\theta = 4.90°$, corresponding to a d_{100}-spacing value of 18.0 Å was present without annealing. But after thermal annealing at 80 °C for 10 min, a slightly increased intensity diffraction peak at $2\theta = 5.28°$ was observed. More importantly, the peak position corresponds to a smaller d_{100}-spacing value of 16.7 Å, which indicating closer packing along the 100 direction. The second-order diffraction peak (200) was clearly observed for DCAO3TCz both without and with thermal annealing, implying a highly organized assembly of this π-conjugated molecule in the solid state. Moreover, the film of DCAO3TCz after thermal annealing showed a stronger second-order diffraction peak than that without thermal annealing. These results indicate that while both small molecule films show better ordered packing after thermal annealing, DCAO3TCz exhibits a better ordered packing with/out annealing than DCAO3TF. This is consistent with the observed higher J_{sc} for DCAO3TCz. As plotted in Fig. 6, the hole mobilities of the films of the two new molecules blended with $PC_{61}BM$ were measured by the SCLC method. The results are summarized in Table 3. The hole mobility of the two molecules are at the range of 10^{-5}–10^{-4} cm^2 V^{-1} s^{-1}, and not very high. After thermal annealing at 80 °C for 10 min, both the molecules blended with $PC_{61}BM$ show a higher hole mobility than those without thermal annealing which could benefit charge transport and thus lead to a higher J_{sc}. Compared with the results of DCAO3TCz, the lower J_{sc} and EQE value of DCAO3TF could be related to the lower hole mobility.

AFM and TEM were used to analyze the morphology of the blend films before and after annealing. As shown in Fig. 7, while the films have a relatively small root mean square (*rms*) roughness before and after annealing, the *rms* roughness of the DCAO3TF/$PC_{61}BM$ film increases from 0.97 to 1.08 nm and that of the DCAO3TCz/$PC_{61}BM$ film decreases from 1.41 to 1.09 nm. From the phase images (Fig. 7e-h), both DCAO3TF/$PC_{61}BM$ and DCAO3TCz/$PC_{61}BM$ blend films after annealing exhibit better interpenetrating network morphology than those without annealing. This is also demonstrated by TEM images (Fig. 8). A good

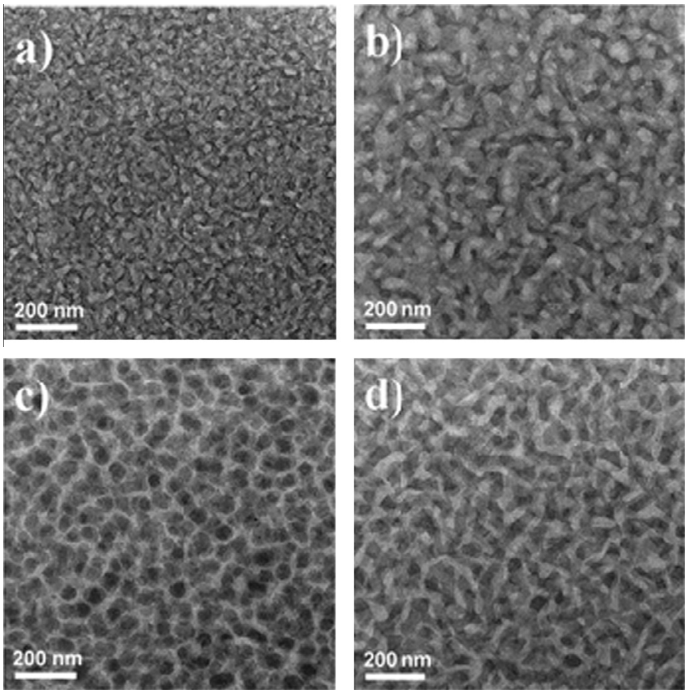

Fig. 8. TEM images of (a and b) DCAO3TF/$PC_{61}BM$ (1:0.8, w/w) and (c and d) DCAO3TF/ $PC_{61}BM$ (1:0.8, w/w) blend films from $CHCl_3$. (a and c) no annealing, (b and d) after annealing at 80 °C for 10 min.

interpenetrating network of donor/acceptor in the blend film could be helpful for exciton diffusion and reduce recombination of exciton. AFM and TEM images also clearly show that the DCAO3TCz/PC_{61}BM blend film has a better interpenetrating network than the DCAO3TF/PC_{61}BM blend film both before and after thermal annealing. Compared with DCAO3TF/PC_{61}BM blend film, the better morphology of films based on DCAO3TCz/PC_{61}BM could lead to a more efficient exciton diffusion and separation and thus higher J_{sc}. Besides, the TEM images also indicate that the unsatisfactory solar cell performance of these two small molecules is to some degree related to the unoptimized morphology of the blend films with PC_{61}BM, as the domain sizes of DCAO3TF/PC_{61}BM and DCAO3TCz/PC_{61}BM blend films are estimated to be 80 and 60 nm, respectively, much larger than the ideal charge diffusion length (10–20 nm) [41–45]. The large domain size of active layer based on these two molecules blended with PC_{61}BM lead to less efficient exciton separation, charge transport, and thus unoptimized J_{sc}.

4. Conclusion

Two new A–D–A structure small molecule donor materials, named DCAO3TF and DCAO3TCz with weak electron-donating units, fluorene and carbazole as the central building blocks were designed and synthesized for high V_{oc} SM-OPV devices. Devices using DCAO3TF achieve a V_{oc} of 1.07 V, which is one of the highest observed for donor:PCBM bulk heterojunction devices. The high V_{oc} was obtained by the low HOMO energy level caused by the central building block fluorene and carbazole units. Their low J_{sc} values are mainly attributed to the large domain size of the donor materials in the active layers. We believe that through further delicate chemical structure design and device optimization, high performance SM-OPV devices with a high V_{oc} may be obtained in the near future.

Acknowledgments

The authors gratefully acknowledge the financial support from MOST (2014CB643502 and 2012CB933401), NSFC (51373078, 21374050 and 51273093), PCSIRT (IRT1257) and Tianjin city (13RCGFGX01121).

Appendix A. Supplementary material

Supplementary data associated with this article can be found, in the online version, at http://dx.doi.org/10.1016/j.orgel.2014.06.012.

References

[1] A.J. Heeger, Chem. Soc. Rev. 39 (2010) 2354–2371.
[2] R. Po, M. Maggini, N. Camaioni, J. Phys. Chem. C 114 (2009) 695–706.
[3] A.C. Arias, J.D. MacKenzie, I. McCulloch, J. Rivnay, A. Salleo, Chem. Rev. 110 (2010) 3–24.
[4] L.M. Chen, Z. Hong, G. Li, Y. Yang, Adv. Mater. 21 (2009) 1434–1449.
[5] D.J. Lipomi, Z. Bao, Energy Environ. Sci. 4 (2011) 3314–3328.
[6] F.C. Krebs, Sol. Energy Mater. Sol. Cells 93 (2009) 394–412.
[7] Y. Lin, H.F. Dam, T.R. Andersen, E. Bundgaard, W. Fu, H. Chen, F.C. Krebs, X. Zhan, J. Mater. Chem. C 1 (2013) 8007–8010.
[8] C. Girotto, D. Cheyns, T. Aernouts, F. Banishoeib, L. Lutsen, T.J. Cleij, D. Vanderzande, J. Genoe, J. Poortmans, P. Heremans, Org. Electron. 9 (2008) 740–746.
[9] H. Zhou, L. Yang, W. You, Macromolecules 45 (2012) 607–632.
[10] M.C. Scharber, D. Muhlbacher, M. Koppe, P. Denk, C. Waldauf, A. Heeger, C. Brabec, Adv. Mater. 18 (2006) 789–794.
[11] F. He, L. Yu, J. Phys. Chem. Lett. 2 (2011) 3102–3113.
[12] Z. He, C. Zhong, S. Su, M. Xu, H. Wu, Y. Cao, Nat. Photon. 6 (2012) 591–595.
[13] S.H. Liao, H.J. Jhuo, Y.S. Cheng, S.A. Chen, Adv. Mater. 25 (2013) 4766–4771.
[14] J. You, L. Dou, K. Yoshimura, T. Kato, K. Ohya, T. Moriarty, K. Emery, C.C. Chen, J. Gao, G. Li, Y. Yang, Nat. Commun. 4 (2013) 1446.
[15] J. Roncali, Acc. Chem. Res. 42 (2009) 1719–1730.
[16] H. Zhou, L. Yang, A.C. Stuart, S.C. Price, S. Liu, W. You, Angew. Chem. Int. Ed. 50 (2011) 2995–2998.
[17] C.M. Amb, S. Chen, K.R. Graham, J. Subbiah, C.E. Small, F. So, J.R. Reynolds, J. Am. Chem. Soc. 133 (2011) 10062–10065.
[18] S. Shen, P. Jiang, C. He, J. Zhang, P. Shen, Y. Zhang, Y. Yi, Z. Zhang, Z. Li, Y. Li, Chem. Mater. 25 (2013) 2274–2281.
[19] L.-Y. Lin, C.-W. Lu, W.-C. Huang, Y.-H. Chen, H.-W. Lin, K.-T. Wong, Org. Lett. 13 (2011) 4962–4965.
[20] H.-W. Lin, J.-H. Chang, W.-C. Huang, Y.-T. Lin, L.-Y. Lin, F. Lin, K.-T. Wong, H.-F. Wang, R.-M. Ho, H.-F. Meng, J. Mater. Chem. A 2 (2014) 3709–3714.
[21] Y. Liu, C.C. Chen, Z. Hong, J. Gao, Y. Yang, H. Zhou, L. Dou, G. Li, Y. Yang, Sci. Rep. 3 (2013).
[22] J. Zhou, Y. Zuo, X. Wan, G. Long, Q. Zhang, W. Ni, Y. Liu, Z. Li, G. He, C. Li, B. Kan, M. Li, Y. Chen, J. Am. Chem. Soc. 135 (2013) 8484–8487.
[23] A. Mishra, P. Bauerle, Angew. Chem. Int. Ed. 51 (2012) 2020–2067.
[24] Y. Chen, X. Wan, G. Long, Acc. Chem. Res. 46 (2013) 2645–2655.
[25] J.E. Coughlin, Z.B. Henson, G.C. Welch, G.C. Bazan, Acc. Chem. Res. 47 (2013) 257–270.
[26] A.K.K. Kyaw, D.H. Wang, D. Wynands, J. Zhang, T.Q. Nguyen, G.C. Bazan, A.J. Heeger, Nano Lett. 13 (2013) 3796–3801.
[27] H.-Y. Lin, W.-C. Huang, Y.-C. Chen, H.-H. Chou, C.-Y. Hsu, J.T. Lin, H.-W. Lin, Chem. Commun. 48 (2012) 8913–8915.
[28] J. Zhou, X. Wan, Y. Liu, G. Long, F. Wang, Z. Li, Y. Zuo, C. Li, Y. Chen, Chem. Mater. 23 (2011) 4666–4668.
[29] J. Zhou, X. Wan, Y. Liu, Y. Zuo, Z. Li, G. He, G. Long, W. Ni, C. Li, X. Su, Y. Chen, J. Am. Chem. Soc. 134 (2012) 16345–16351.
[30] G. He, Z. Li, X. Wan, Y. Liu, J. Zhou, G. Long, M. Zhang, Y. Chen, J. Mater. Chem. 22 (2012) 9173–9180.
[31] N. Blouin, A. Michaud, D. Gendron, S. Wakim, E. Blair, R. Neagu-Plesu, M. Belletête, G. Durocher, Y. Tao, M. Leclerc, J. Am. Chem. Soc. 130 (2007) 732–742.
[32] M. Svensson, F. Zhang, S.C. Veenstra, W.J.H. Verhees, J.C. Hummelen, J.M. Kroon, O. Inganäs, M.R. Andersson, Adv. Mater. 15 (2003) 988–991.
[33] J. Li, A.C. Grimsdale, Chem. Soc. Rev. 39 (2010) 2399–2410.
[34] S.H. Park, A. Roy, S. Beaupre, S. Cho, N. Coates, J.S. Moon, D. Moses, M. Leclerc, K. Lee, A.J. Heeger, Nat. Photon. 3 (2009) 297–302.
[35] J. Zhang, W. Cai, F. Huang, E. Wang, C. Zhong, S. Liu, M. Wang, C. Duan, T. Yang, Y. Cao, Macromolecules 44 (2011) 894–901.
[36] J.F. Morin, M. Leclerc, Macromolecules 35 (2002) 8413–8417.
[37] J.F. Morin, M. Leclerc, Macromolecules 34 (2001) 4680–4682.
[38] W.J.E. Beek, M.M. Wienk, M. Kemerink, X. Yang, R.A.J. Janssen, J. Phys. Chem. B 109 (2005) 9505–9516.
[39] G. Long, X. Wan, B. Kan, Y. Liu, G. He, Z. Li, Y. Zhang, Y. Zhang, Q. Zhang, M. Zhang, Y. Chen, Adv. Energy Mater. 3 (2013) 639–646.
[40] Z. Li, G. He, X. Wan, Y. Liu, J. Zhou, G. Long, Y. Zuo, M. Zhang, Y. Chen, Adv. Energy Mater. 2 (2012) 74–77.
[41] P. Peumans, A. Yakimov, S.R. Forrest, J. Appl. Phys. 93 (2003) 3693–3723.
[42] S.R. Cowan, N. Banerji, W.L. Leong, A.J. Heeger, Adv. Funct. Mater. 22 (2012) 1116–1128.
[43] G. Garcia-Belmonte, A. Munar, E.M. Barea, J. Bisquert, I. Ugarte, R. Pacios, Org. Electron. 9 (2008) 847–851.
[44] X. Yang, J. Loos, S.C. Veenstra, W.J.H. Verhees, M.M. Wienk, J.M. Kroon, M.A.J. Michels, R.A.J. Janssen, Nano Lett. 5 (2005) 579–583.
[45] C.M. Proctor, M. Kuik, T.Q. Nguyen, Prog. Polym. Sci. 38 (2013) 1941–1960.